Energy-Sink Analysis for Asymmetric Dual-Spin Spacecraft

T. M. SPENCER*
Ball Brothers Research Corporation, Boulder, Colo.

Energy-sink analysis has been widely used to investigate the nutational stability of spin-stabilized spacecraft. The familiar stability condition for dual-spin spacecraft does not give correct results for an asymmetric platform. This condition is generalized by replacing the average platform and rotor nutation frequencies and energy dissipation rates with time-varying quantities. (The generalized "nutation frequency" is the rotation rate of the transverse angular momentum vector.) For a satellite with a despun asymmetric platform, the generalized condition suggests that the geometric (rather than algebraic) mean transverse moment of inertia is a crucial stability parameter.

Nomenclature

$\mathbf{X}_1, \mathbf{X}_2, \mathbf{X}_3$ = platform-fixed coordinate frame
$\mathbf{H}, h$ = angular momentum vector and its magnitude
$\boldsymbol{\Omega}$ = angular velocity vector
$\mathbf{M}$ = disturbance torque vector
I_s = rotor spin axis moment of inertia
I_t = over-all transverse moment of inertia
$\mathbf{S}$ = spin-bearing axis
$\mathbf{H}_s, h_s$ = spin-angular momentum and its magnitude
$\mathbf{H}_t, h_t$ = transverse angular momentum and its magnitude
$\boldsymbol{\Omega}_t, \omega_t$ = transverse angular velocity vector and its magnitude
$\boldsymbol{\Omega}_s, \omega_s$ = spin-angular velocity vector and its magnitude
$\Delta\omega_s$ = change in spin speed
ω^I = inertial nutation frequency
ω^P = platform-fixed nutation frequency
ω^R = rotor-fixed nutation frequency
θ = nutation coning half angle
$\dot{T}^R$ = rotor energy dissipation rate
I_1, I_2 = minimum and maximum over-all transverse moments of inertia
ω_1, ω_2 = transverse angular velocities about the $\mathbf{X}_1$ and $\mathbf{X}_2$ axes
ω_0 = initial value of ω_2
$\hat{\omega}$ = average inertial nutation frequency
ϕ^Ω = central angle from $\mathbf{X}_2$ to $\boldsymbol{\Omega}_t$
ϕ^s = central angle from $-\mathbf{X}_2$ to $\mathbf{S}$ (also the nutation angle)
I_t = effective instantaneous transverse moment of inertia
θ^Ω = coning half angle of $\boldsymbol{\Omega}$ about $\mathbf{H}$
θ^s = coning half angle of $\mathbf{S}$ about $\mathbf{H}$
h_1, h_2 = transverse angular momenta magnitudes about the $\mathbf{X}_1$ and $\mathbf{X}_2$ axes
T = kinetic energy
t = time
K = damping coefficient

Introduction

A DUAL-SPIN spacecraft is spin-stabilized by a single rotor or inertia wheel. The platform can be totally or partially despun about the rotor spin axis by a despin servo which generates interbody torques. This stabilization technique was used on rod-shaped sounding rockets in the early 50's and was first used for satellites on the disk-shaped Orbiting Solar Observatory 1 in 1962. Recently, the technique has been widely used for both rod-shaped and disk-shaped satellites.

A disk-shaped dual-spin satellite is unconditionally stable in the presence of energy dissipation on the rotor. In 1964 Landon and Stewart showed that a symmetric rod-shaped dual-spin satellite could also be stabilized by a passive mechanical nutation damper.[1] In addition to using a damper reaction-torque calculation, they used an "energy-sink" analysis similar to that previously applied to single spinning bodies by Thompson and Reiter.[2] The stability condition is often expressed, in a form given in 1965 by Iorillo,[3] as a comparison of the ratio of the energy dissipation rate to the nutation frequency on the platform, to that ratio on the rotor.

In 1967, Likins[4] extended the energy-sink stability condition for satellites with asymmetric platforms with the provision that the dissipation rates and nutation frequencies be separately averaged. In 1972, two papers questioned this condition.[5,6] In the first paper, Cherchas and Hughes showed that for a satellite with a despun asymmetric platform, the geometric mean transverse moment of inertia is the crucial stability quantity. They suggested that the inherent lack of rigor in the energy-sink method may have misled Likins to his conclusion that the algebraic mean is the crucial quantity. In the second paper, the present author showed that a refined version of the energy-sink condition also supports the importance of the geometric mean.[6] The refined condition is not as easy to apply as the existing condition because intercycle variations (as well as average energy dissipation rates) must be determined.

Energy-sink analyses continue to be widely used to predict spin axis behavior and to explain flight anomalies.[7-11] This is partly because the method is applicable for nonlinear effects which are difficult, if not impossible, to treat using more rigorous methods. In any case, it is easier to estimate or measure the energy dissipation rates of a nutating assembly than to determine its over-all dynamic interaction. In spite of continuing advancements in applying other analysis methods, energy-sink analysis will probably remain popular. Its most important limitation may be its inability to assess the effects of changes in the inertia dyadic; an example is given in Ref. 6.

The purpose of this paper is to present and justify the refined energy-sink stability condition which was announced in Ref. 6. Sample digital computer simulations are included here. For completeness, we first review the derivation for a symmetric dual-spin satellite.

Background

The attitude dynamics of a dual-spin satellite are described by the Euler moment equation

$$\dot{\mathbf{H}} + (\boldsymbol{\Omega} \times \mathbf{H}) = \mathbf{M} \tag{1}$$

generalized for a two-body satellite. $\mathbf{H}$, $\boldsymbol{\Omega}$, and $\mathbf{M}$ are the inertial angular momentum, angular rate, and external torque vectors resolved in platform coordinates. In general, external torques cause the momentum vector to "precess" and misalignment of the principal moment of inertia axes causes the spin axis to "wobble." In the sequel, we restrict our attention to the external-

Presented as Paper 73-909 at the AIAA Guidance and Control Conference, Key Biscayne, Fla., August 20–22, 1973; submitted August 27, 1973; revision received March 8, 1974.
Index category: Spacecraft Attitude Dynamics and Control.
* Staff Scientist. Member AIAA.

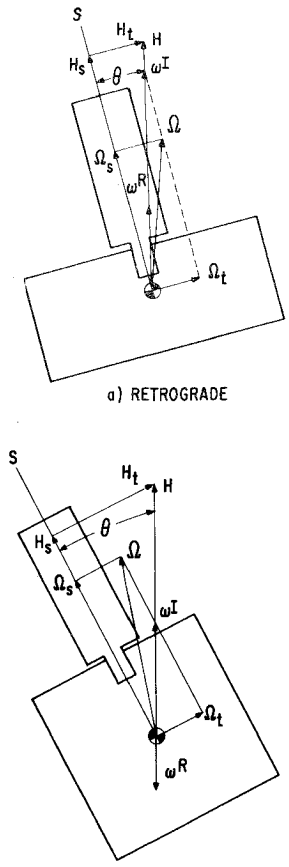

Fig. 1 Nutation of a symmetric spacecraft.

torque-free "nutation" of a perfectly balanced satellite.† To simplify the presentation, we further restrict our attention to a completely despun platform and a symmetric rotor (that is, one with equal transverse moments of inertia).

Under these assumptions, nutation takes the form of a coning motion of the despin bearing axis (simply called the spin axis hereafter) about the angular momentum vector. Without energy dissipation, the nutation cone has an elliptical cross section. The eccentricity depends on the ratio of the platform transverse moments of inertia. Nutational stability is determined by whether energy dissipation causes the average coning angle to grow or decay. Except for an isolated special relationship between the rotor spin and over-all transverse moments of inertia, the total rotational kinetic energy of the satellite changes with the average coning angle. *Energy-sink* stability analyses are based on this correlation. Although the total kinetic energy is independent of the coning angle for an "inertially spherical" satellite, a modified version of the familiar energy-sink approach can still be applied.[1,2]

While rigorous *energy-change* analyses are undoubtedly possible, traditionally simplifying approximations are used. These approximations include the assumption that a hypothetical "constant-energy" nutational motion drives energy dissipators. The energy dissipation rates are estimated without regard for the "direct" effect of the dissipators on the hypothesized motion. The rate of change of the average cone angle is calculated on the basis of the resulting changes in platform and rotor kinetic energy. When these assumptions are justified, nutational behavior can be quickly assessed (even for relatively complicated nonlinear dissipators).

The analysis is especially simple for a symmetric satellite. The constant-energy nutation cone has a constant half angle θ. The relationships among the spin axis **S**, angular momentum vector **H**, and angular velocity vector $\boldsymbol{\Omega}$ are shown schematically in Fig. 1. These vectors are broken into "spin" and "transverse" components. The transverse angular velocity $\boldsymbol{\Omega}_t$ and momentum $\mathbf{H}_t$ are coplanar with **H** and they rotate at a constant rate. The spin and transverse angular momentum magnitudes are

$$h_s = I_s\omega_s \qquad h_t = I_t\omega_t \tag{2}$$

Where I_s is the rotor spin moment of inertia, I_t is the over-all transverse inertia, and ω_s is the rotor spin rate. A fundamental distinction between single-spin and dual-spin satellites is the existence of the two body-fixed nutation frequencies

$$\omega^P = \omega^I = (I_s/I_t)\omega_s$$
$$\omega^R \approx \omega^I - \omega_s = [(I_s - I_t)/I_t]\omega_s \tag{3}$$

where ω^P for the platform is equal to the inertial nutation frequency (for a completely despun platform) and ω^R is the rotor-fixed frequency (to first order in the coning angle θ).

The nutation half angle is

$$\tan\theta = h_t/h_s = (I_t/I_s)(\omega_t/\omega_s) \tag{4}$$

If $I_s > I_t$ then $\omega^I > \omega_s$ and $\omega^R > 0$. This is called "retrograde" nutation. In retrograde nutation the rotor spins with a lower frequency than ω^I. The reverse is true for the "prograde" nutation of a rod-shaped spacecraft.

The difference in the sense of rotor-fixed nutation led to Landon's first and elegantly simple reaction torque stability argument that a rotor-mounted circular constraint damper driven at the inertial nutation frequency would "spin-up" the rotor and therefore stabilize a disk-shaped spacecraft. The reverse is true for a rod-shaped spacecraft. The platform-fixed nutation always has the same sense as rotor spin so a platform-mounted damper tries to stabilize both rod and disk-shaped spacecraft.

In reviewing the energy-sink stability condition we simplify the algebra by ignoring the always stabilizing effect of energy dissipation on the platform and concentrate on the effect of a rotor energy dissipation rate $\dot{T}^R$. In the absence of external torques the magnitude of the angular momentum is constant and the familiar existing stability condition is obtained by solving

$$\tfrac{1}{2}d/dt(\mathbf{H}\cdot\mathbf{H}) = I_t^2\omega_t\dot{\omega}_t + I_s^2\omega_s\dot{\omega}_s = 0$$
and
$$\dot{T}^R = I_t\omega_t\dot{\omega}_t + I_s\omega_s\dot{\omega}_s \tag{5}$$

simultaneously to obtain

$$\omega_t\dot{\omega}_t = I_s\dot{T}^R/I_t(I_s - I_t) \tag{6}$$

and

$$\omega_s\dot{\omega}_s = -I_t\dot{T}^R/I_s(I_s - I_t) \tag{7}$$

Usually only the equation for $\omega_s\dot{\omega}_s$ is used.[4] From Eqs. (3) and (7), the stability condition is expressed in the form

$$-I_s\dot{\omega}_s = \dot{T}^R/\omega^R < 0 \tag{8}$$

where $\dot{T}^R$ is to be averaged over a nutation cycle. The equivalence of Landon's reaction torque and energy-sink approaches is clear from the fact that the left-hand quantity is the net spin-axis reaction torque applied to the rotor. A spin-up torque is clearly required for stability. Because $\dot{T}^R$ is negative for an energy *sink*, ω^R must be positive (retrograde) for stability.

Equation (6) leads to the condition

$$I_t\dot{\omega}_t = \frac{I_s\dot{T}^R}{(I_s - I_t)\omega_t}\left(\frac{I_t\omega_s}{I_t\omega_s}\right) = \left(\frac{\dot{T}^R}{\omega^R}\right)\left(\frac{I_s\omega_s}{I_t\omega_t}\right)$$
$$= \left(\frac{\dot{T}^R}{\omega^R}\right)\left(\frac{1}{\tan\theta}\right) < 0 \tag{9}$$

The two conditions as applied to ω^R are equivalent since $\tan\theta$ is positive by definition. The second condition means that the average transverse reaction torque must be negative. A transverse rate-reducing torque is also clearly necessary for stability.

Nutation for an Asymmetric Despun Platform

For an asymmetric platform, the constant-energy nutation cone has elliptical cross section. The upright ellipse in Fig. 2 represents the path followed by the spin-axis **S**. The total angular

† These modifications of classical nomenclature are used throughout this paper.

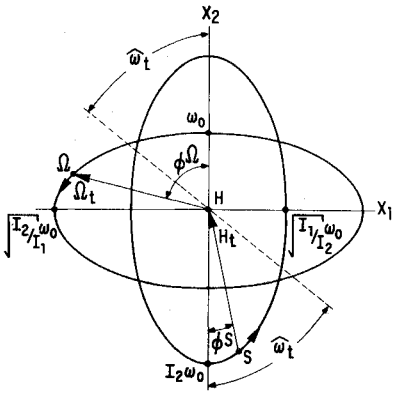

Fig. 2 Nutation for an asymmetric platform ($I_2 > I_1$).

momentum vector **H** is at the origin. The horizontal ellipse represents the path followed by the angular velocity vector **Ω**. These vectors do not remain coplanar and their rotation rates are not constant. To better describe the complex motion we use Likins' solution to the linearized equations (specialized for a despun platform).[4] The solution is

$$\begin{aligned} \omega_1 &= -\omega_0(I_2 I_1)^{1/2} \sin \hat{\omega} t \\ \omega_2 &= \omega_0 \cos \hat{\omega} t \\ \omega_s &= \text{constant} \end{aligned} \tag{10}$$

where ω_1 and ω_2 are inertial transverse rates resolved along axes $\mathbf{X}_1$ and $\mathbf{X}_2$ which are parallel to the platform principal axes but which pass through the combined satellite center of mass, I_1 and I_2 are over-all transverse moments of inertia about axes $\mathbf{X}_1$ and $\mathbf{X}_2$, ω_0 is the initial transverse rate (assumed to be along axis $\mathbf{X}_2$), and

$$\hat{\omega} = [I_s/(I_1 I_2)^{1/2}]\omega_s \tag{11}$$

is the *mean* platform nutation frequency in terms of rotor spin rate ω_s and spin inertia I_s.

Figure 2 contains a schematic representation of the motion of transverse rate vector $\boldsymbol{\Omega}_t = \omega_1 \bar{\mathbf{i}} + \omega_2 \bar{\mathbf{j}}$. This vector is the $\mathbf{X}_1\mathbf{X}_2$ projection of the total angular velocity **Ω** of the rotor. The locus is an ellipse elongated along the platform $\mathbf{X}_1$ axis. The major-to-minor axis ratio is $(I_2/I_1)^{1/2}$ (we assume $I_2 > I_1$ without loss of generality).

The rate of rotation of the $\boldsymbol{\Omega}_t$ vector in the $\mathbf{X}_1\mathbf{X}_2$ plane is not constant. The central angle measured from axis $\mathbf{X}_2$ to $\boldsymbol{\Omega}_t$ is

$$\phi^{\Omega} = \tan^{-1}(-\omega_1/\omega_2) = \tan^{-1}[(I_2/I_1)^{1/2} \tan \hat{\omega} t] \tag{12}$$

in view of Eq. (10). Differentiation yields the rotation rate as

$$\begin{aligned} \dot{\phi}^{\Omega} &= \frac{(I_2/I_1)^{1/2}\hat{\omega} \sec^2 \hat{\omega} t}{1+(I_2/I_1)\tan^2 \hat{\omega} t} \\ &= \frac{I_s \omega_s}{I_2 \sin^2 \hat{\omega} t + I_1 \cos^2 \hat{\omega} t} \\ &= \frac{I_s \omega_s}{I_t[\hat{\omega} t + (\pi/2)]} \end{aligned} \tag{13}$$

where use is made of Eq. (11) and I_t is the instantaneous transverse inertia about a line (the dashed line in Fig. 2) that is aligned with $\mathbf{X}_2$ at $t = 0$ and that rotates at the constant rate $\hat{\omega}$. That is

$$I_t(\hat{\omega} t) = I_1 \sin^2 \hat{\omega} t + I_2 \cos^2 \hat{\omega} t \tag{14}$$

The time-varying cone angle of the rotor angular velocity vector **Ω** about **H** is

$$\tan \theta^{\Omega} = \omega_t/\omega_s = (\omega_1{}^2 + \omega_2{}^2)^{1/2}/\omega_s = \omega_0/\omega_s[I_t(\hat{\omega} t + \pi/2)/I_1]^{1/2} \tag{15}$$

where ω_t is the magnitude of $\boldsymbol{\Omega}_t$ and use has been made of Eqs. (10) and (11).

Figure 2 also depicts the locus of the *tail* of the transverse momentum vector $\mathbf{H}_t$. The ellipses are drawn to the same scale for convenience of representation. The tip of $\mathbf{H}_t$ is at **H** instead of **S** for reasons that are clear from Fig. 1. The locus is also that of the spin axis **S**. The locus is an ellipse of the same shape as the transverse rate ellipse but elongated along the $\mathbf{X}_2$ instead of the $\mathbf{X}_1$ axis. The transverse rate and the momentum vectors have the same direction when $\boldsymbol{\Omega}_t$ is along the $\mathbf{X}_1$ and $\mathbf{X}_2$ axes. At intermediate points the vectors are not colinear. The misalignment is caused by the difference in transverse inertias for the same reason that **H** and **Ω** are not colinear in Fig. 1.

The instantaneous spin-axis *nutation angle* is defined as the central angle ϕ^s from the $-\mathbf{X}_2$ axis to **S** (see Fig. 2). In analogy with Eq. (12) we have

$$\begin{aligned} \phi^s &= \tan^{-1}(-h_1/h_2) = \tan^{-1}(-I_1\omega_1/I_2\omega_2) \\ &= \tan^{-1}[I_1(I_2/I_1)^{1/2}\omega_0 \sin \hat{\omega} t / I_2 \omega_0 \cos \hat{\omega} t] \\ &= \tan^{-1}[(I_1/I_2)^{1/2} \tan \hat{\omega} t] \end{aligned} \tag{16}$$

where h_1 and h_2 are the transverse angular momentum magnitudes along $\mathbf{X}_1$ and $\mathbf{X}_2$.

The instantaneous inertial spin-axis nutation rate (classically the precession rate) is

$$\begin{aligned} \dot{\phi}^s &= \frac{(I_1/I_2)^{1/2}\hat{\omega} \sec^2 \hat{\omega} t}{1+(I_1/I_2)\tan^2 \hat{\omega} t} \\ &= \frac{I_s \omega_s}{I_1 \sin^2 \hat{\omega} t + I_2 \cos^2 \hat{\omega} t} \\ &= \frac{I_s \omega_s}{I_t(\hat{\omega} t)} \end{aligned} \tag{17}$$

in analogy with Eq. (13).

Equations (13) and (17) are time-varying generalizations of the inertial nutation rate given in Eq. (3) for a symmetric satellite. We will use the symbol ω^I for the spin-axis coning rate in Eq. (17). To first order in θ^s the magnitude of the rotor-fixed nutation rate is then

$$\omega^R \approx \omega^I - \omega_s = [(I_s - I_t)/I_t]\omega_s \tag{18}$$

where we write I_t in place of $I_t(\hat{\omega} t)$.

The variations in both nutation rates, the transverse rate and $\dot{\phi}^s$ are described through variation of I_t. The ratio of the maximum to the minimum platform-fixed nutation rate is I_2/I_1. We will be most interested in values of I_s between I_2 and I_1. For this condition, the rotor-fixed rate changes sign every quarter platform-fixed nutation cycle and

$$\omega^R(0)/\omega^R(\pi/2) = (I_s - I_2)(I_1)/(I_2)(I_s - I_1) \tag{19}$$

Figure 3 shows the variations, over a quarter of a platform nutation cycle, of I_t, ω^R, and $\int_0^t \omega^R dt$ for the special case $I_s = (I_1 I_2)^{1/2}$. In this case, the rotor spin rate is equal to the mean nutation frequency $\hat{\omega}$ and we call the motion "neutral" nutation. (Notice that ω^R integrates to zero over each quarter cycle). A 10:1 ratio of I_2/I_1 is used to clearly show the nature of the variations. While mathematically proper, this ratio can only be as large as 4:1 for a real spacecraft with $I_s = (I_1 I_2)^{1/2}$.

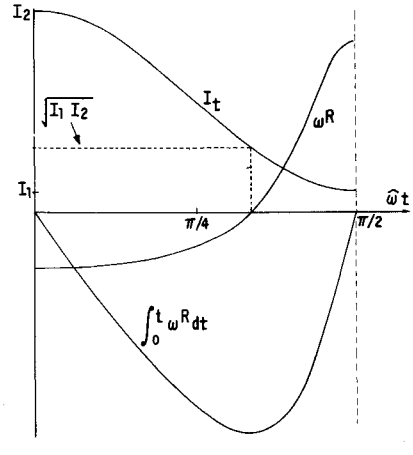

Fig. 3 "Neutral" nutation for $I_s = (I_1 I_2)^{1/2}$.

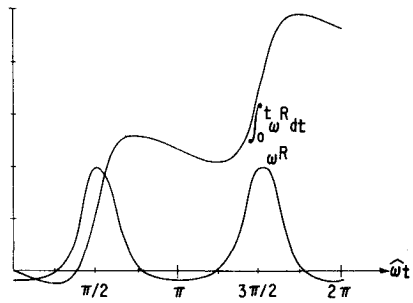

Fig. 4 Retrograde nutation for $I_s = (I_1+I_2)/2$.

If $I_s \neq (I_1I_2)^{1/2}$, then $\omega_s \neq \hat{\omega}$ and a "bias" component is added to the cyclical (zero average) rotor-resolved nutation rate. This bias is retrograde or prograde compared to ω_s depending on whether $I_s > (I_1I_2)^{1/2}$ or $I_s < (I_1I_2)^{1/2}$, respectively.

Figures 4 and 5 show the variations of ω^R and $\int_0^t \omega^R dt$ over a full inertial nutation cycle for cases where

$$I_s = (I_1+I_2)/2$$

and

$$I_s = 2I_1I_2/(I_1+I_2)$$

respectively. Because

$$(I_1+I_2)/2 > (I_1I_2)^{1/2} > 2I_1I_2/(I_1+I_2) \quad \text{for} \quad I_1 \neq I_2$$

we get a retrograde bias in Fig. 4 and a prograde bias in Fig. 5. (That is, the spin axis is nutating faster than the rotor is spinning in Fig. 4 and slower in Fig. 5.)

These moments of inertia are, respectively, the algebraic, geometric, and harmonic mean transverse inertias. They have special significance in treating the effects of high-frequency variations in ω^R caused by various forms of energy dissipation.

The variations depicted in Figs. 3–5 are *constant-energy* variations. (Actually, they are first-order approximations in ω_0/ω_s.) To arrive at the desired stability condition we must assess the effect of rotor-energy dissipation. However, the nature of the constant-energy nutational motions already suggests that the stability boundary is defined by $I_s = (I_1I_2)^{1/2}$.

Refined Stability Condition

To derive the stability conditions for a dual-spin spacecraft with a rigid despun asymmetric platform, we develop the relationship between a rotor energy dissipation rate $\dot{T}^R$ and $\dot{\omega}_0$ and $\dot{\omega}_s$, to first order in ω_0/ω_s and in $\Delta\omega_s/\omega_s$. The resulting conditions are applicable for sufficiently small nutation angles and for sufficiently small energy dissipation rates. The same restrictions apply to the familiar conditions for a symmetric spacecraft but second-order expressions do not appear as dramatically in the derivation.

The derivation is based on the solutions in Eqs. (10) to the linearized equations of motion. Differentiating with respect to time yields

$$\begin{aligned}\dot{\omega}_1 &= -\dot{\omega}_0(I_2/I_1)^{1/2}\sin\hat{\omega}t - \omega_0(I_2/I_1)^{1/2}(\hat{\omega}+t\dot{\hat{\omega}})\cos\hat{\omega}t\\ \dot{\omega}_2 &= \dot{\omega}_0\cos\hat{\omega}t - \omega_0(\hat{\omega}+t\dot{\hat{\omega}})\sin\hat{\omega}t\\ \dot{\omega}_s &= \dot{\omega}_s\end{aligned} \tag{20}$$

From Eqs. (10, 14, and 20) the momentum magnitude conservation condition can be expressed as

$$\begin{aligned}\tfrac{1}{2}d/dt(\mathbf{H}\cdot\mathbf{H}) &= I_1{}^2\omega_1\dot{\omega}_1 + I_2{}^2\omega_2\dot{\omega}_2 + I_s{}^2\omega_s\dot{\omega}_s =\\ &I_2I_t\omega_0\dot{\omega}_0 + I_s{}^2\omega_s\dot{\omega}_s +\\ &\omega_0{}^2(I_1-I_2)I_2(\hat{\omega}+t\dot{\hat{\omega}})(\sin\hat{\omega}t)(\cos\hat{\omega}t) \approx\\ &I_2I_t\omega_0\dot{\omega}_0 + I_s{}^2\omega_s\dot{\omega}_s = 0\end{aligned} \tag{21}$$

to first order in ω_0/ω_s and for sufficiently small t (that is, for sufficiently small $\Delta\omega_s/\omega_s$). The kinetic energy rate expression is

$$\begin{aligned}\dot{T}^R &= I_1\omega_1\dot{\omega}_1 + I_2\omega_2\dot{\omega}_2 + I_s\omega_s\dot{\omega}_s\\ &= I_2\omega_0\dot{\omega}_0 + I_s\omega_s\dot{\omega}_s\end{aligned} \tag{22}$$

Simultaneous solution of Eqs. (21) and (22) yields

$$\omega_0\dot{\omega}_0 = I_s\dot{T}^R/I_2(I_s-I_t) \tag{23}$$

and

$$\omega_s\dot{\omega}_s = -I_t\dot{T}^R/I_s(I_s-I_t) \tag{24}$$

These are the same as Eqs. (6) and (7) for the symmetric satellite except that I_t is the varying instantaneous transverse inertia from Eq. (14) and that I_2 appears in place of I_t in the equation for $\omega_0\dot{\omega}_0$. (I_1 would appear in place of I_2 if the initial transverse rate were aligned with the $\mathbf{X}_1$ instead of the $\mathbf{X}_2$ axis.) Using Eq. (18) and integrating Eqs. (23) and (24) over an appropriate time interval we obtain the desired stability conditions

$$-I_s\int_{t_1}^{t_2}\dot{\omega}_s\,dt = \int_{t_1}^{t_2}(\dot{T}^R/\omega^R)\,dt < 0 \tag{25}$$

and

$$I_t\int_{t_1}^{t_2}\dot{\omega}_0\,dt = I_s\omega_s/I_2\omega_0\int_{t_1}^{t_2}(\dot{T}^R/\omega^R)\,dt = 1/\tan\theta^s(0)\int_{t_1}^{t_2}(\dot{T}^R/\omega^R)\,dt < 0 \tag{26}$$

The expression in Eq. (25) can be viewed as an estimate of the spin-axis torque impulse applied to the rotor by the energy dissipators. Because ω^R varies with time for an asymmetric platform, it is not possible to separately integrate numerator and denominator. In effect, Likins did this in arriving at his erroneous stability conclusion.[4] Because I_t varies, Eq. (26) can be viewed as containing a "weighted" transverse torque impulse estimate.

The coefficient of $\dot{T}^R$ in Eqs. (25) and (26) is a time-varying intercycle weighting factor. The need to take account of this factor is the principal stability contribution of this paper. To do this, $\dot{T}^R$ variations must be determined before averaging can be used to get the stability result. This may require a complete determination of the motion of a specific damper. A first-order solution of the damper-satellite equations would be consistent with the inherent energy-sink approximations. Unfortunately, the solution is more complicated for an asymmetric satellite than the symmetric example in Ref. 11. Furthermore, the appropriate time interval for averaging is not as clearly defined.

The following observations can be made without explicitly determining $\dot{T}^R$. If $I_2 > I_s > I_1$ and $\omega_1(o) = 0$, then $I_t > I_s$ near $t = 0$. For this initial phasing, because $\dot{T}^R$ is always negative, the first portion of the first quarter of a platform-fixed nutation cycle is a destabilizing interval. The portion following the point where $I_s = I_t$ is a stabilizing interval. This boundary point is the point where $I_t = I_s$. For the case where $I_s = (I_1I_2)^{1/2}$, Fig. 3 shows how the reciprocal of the weighting factor varies.

We can get an idea of how ω_s changes by assuming $\dot{T}^R = -K(\omega^R)^2$ for a rotor-fixed "viscous energy-sink." We will treat K as a constant although variations are expected.[13] Near-resonance linear damping gives higher power variation with ω^R. Also, variation is expected with ω_0 and with the difference between $\hat{\omega}t$ and $\omega_s t$. These variations are functions of damper parameters including its mounting geometry in the rotor and will not be treated in this paper.

For our simplified $\dot{T}^R$ model, Eq. (24) becomes

$$\dot{\omega}_s = K/I_s(\omega^R) \tag{27}$$

This suggests that the behavior of ω_s and $\int_0^t \omega^R dt$ are similar. Over regions of small (or zero-averaged) variation of K, Eq. (27)

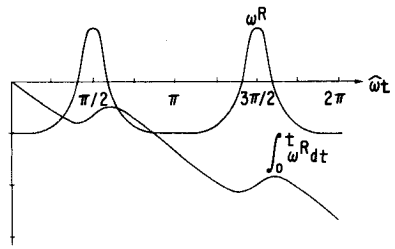

Fig. 5 Prograde nutation for $I_s = 2I_1I_2/(I_1+I_2)$.

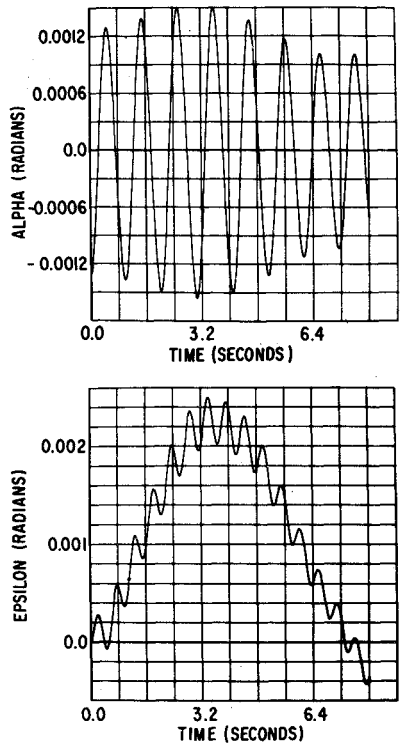

Fig. 6 Change in "barely" retrograde nutation for coulomb rotor damping.

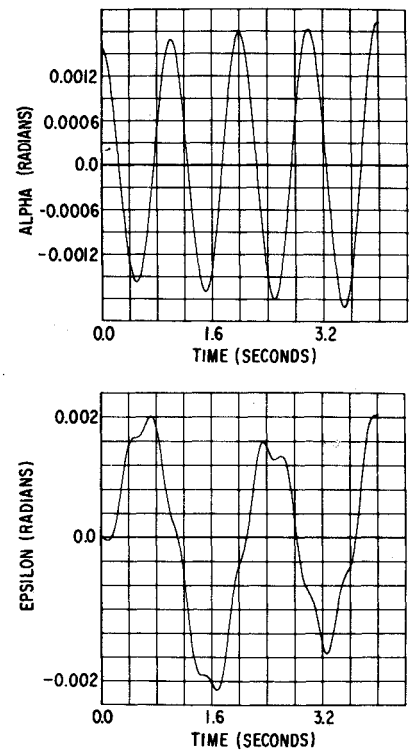

Fig. 7 Change in prograde nutation for coulomb rotor damping.

predicts average growth of ω_s (i.e., stability) for a retrograde bias in rotor-fixed nutation. This is equivalent to $I_s > (I_1 I_2)^{1/2}$.

If coulomb damping or if higher power rate damping coefficients are assumed and if the integration interval is a quarter of an *inertial* nutation cycle, results differ. For continuous coulomb damping (i.e., no sticking), Eq. (25) only predicts ω_s growth for $I_s > (I_1 + I_2)/2$. For sufficiently low adhesion threshold rates, Eq. (25) predicts growth of ω_s for smaller values of I_s. For damping proportional to higher powers of relative rate, ω_s growth is predicted for values of I_s slightly smaller than $(I_1 I_2)^{1/2}$.

For more precise results, $\dot{T}^R$ must be more precisely determined, changes in ω^R must be reflected in the $\dot{T}^R$ expression, and the integration interval must be extended. Except for the effect of coulomb damping, our simplified $\dot{T}^R$ estimates corroborate the assertion that $I_s = (I_1 I_2)^{1/2}$ is the stability boundary. The results for coulomb damping can be explained from the nutation behavior in Fig. 6. The computer run predicts alternate growth and decay depending on the phasing of the low-frequency rotor-fixed nutation component. These phase changes are caused by changes in the alignment of the simulated energy dissipation mechanism with respect to the transverse rate vector. These changes are not incorporated in our simplified energy-sink estimate.

Corroborating Computer Simulations

A digital computer simulation, which uses first-order approximations to the exact equations of motion, was used to show how a rotor-mounted inertia sphere changes nutation for different values of I_s. The inertia sphere is gimbaled about a single rotor-fixed transverse axis. The gimbal is damped by coulomb friction in each of the runs presented.

For slightly retrograde nutation, Fig. 6 shows initial growth of the spin-axis Euler angle ALFA. This is followed by greater decay so that there is a net nutation decay. This value of I_s is barely larger than the geometric mean transverse inertia and approximately defines the stability boundary. The gimbal angle plot (EPSILON) clearly shows both a high-frequency cyclical variation and the low-frequency "bias" component in ω^R. (The bias in the nutation magnitude appears as a sinusoid in the rotor-fixed gimbal.) The gimbal rate is dominated by the higher frequency motion. However, the effects of the higher frequency energy changes are effectively averaged out of the ALFA motion. This run shows only a half cycle of the lower frequency

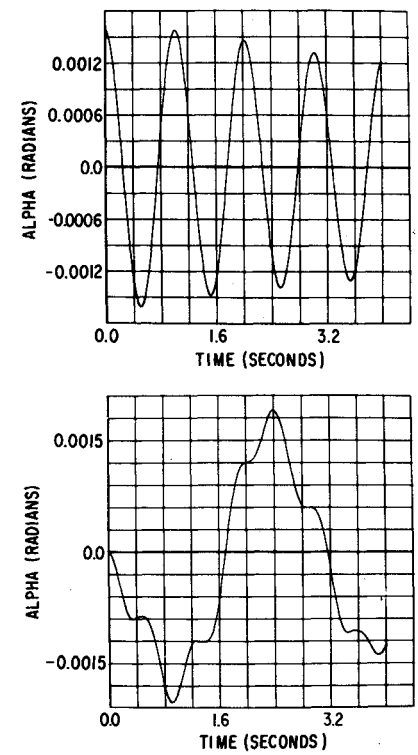

Fig. 8 Change in retrograde nutation for coulomb rotor damping.

nutation angle variation. This frequency is the difference between $\hat{\omega}$ and ω_s. Runs simulating viscous, quadratic, and cubic gimbal damping gave similar results.

Because nutation alternately grows and decays, it is clear that great care must be used in applying any kind of analytical stability results. In particular, it is clear that the analysis must span a sufficient time interval.

Figure 7 shows nutation growth for prograde nutation. I_s is just larger than the reduced transverse inertia. The gimbal motion is dominated by the bias component of ω^R (resolved along the gimbal axis). The growth rate varies slightly because of imperfect averaging of the gimbal torques, but the "integration interval" is clearly long enough to give the proper trend.

Figure 8 shows nutation decay for retrograde nutation. I_s is just below the algebraic mean transverse inertia. Decay is rather steady. The conditions for runs 6–8 are the same except that I_s was changed and ω_s was changed to give equal momentum.

Notice the phase difference in the gimbal motion, initially going positive in Fig. 7 and negative in Fig. 8. This occurs because the rotor-fixed nutation is prograde in Fig. 7 and retrograde in Fig. 8. The computer results corroborate the contention that the stability boundary is for $\hat{\omega} = \omega_s$ [that is, for $I_s = (I_1 I_2)^{1/2}$].

Conclusion

For a despun platform, platform asymmetries produce an elliptical nutational coning motion. The familiar energy-sink stability condition is revised by defining a generalized time varying nutation frequency. Refined energy dissipation rate estimates are required for accurate assessment of stability. For a simplified estimate, the refined condition shows that the geometric mean transverse moment of inertia is a crucial stability parameter. For generalized concepts of prograde and retrograde nutation, this result is consistent with the well-known result for symmetric satellites. The result is corroborated by digital computer simulations.

References

[1] Landon, V. D. and Stewart, B., "Nutational Stability of an Axisymmetric Body Containing a Rotor," *Journal of Spacecraft and Rockets*, Vol. 1, No. 6, Nov.–Dec. 1964, pp. 682–684.

[2] Reiter, G. S. and Thompson, W. T., "Rotational Motion of Passive Space Vehicles," presented as Paper 62-42 at the AAS Goddard Memorial Symposium, Greenbelt, Md., March 1962.

[3] Iorillo, A. J., "Nutation Damping Dynamics of Axisymmetric Rotor Stabilized Satellites," presented at the ASME Winter Meeting, Chicago, Ill., Nov. 1965.

[4] Likins, P. W., "Attitude Stability for Dual Spin Spacecraft," *Journal of Spacecraft and Rockets*, Vol. 4, No. 12, Dec. 1967, pp. 1638–1643.

[5] Chercas, D. B. and Hughes, P. C., "Attitude Stability of a Dual-Spin Satellite with a Large Flexible Solar Array," *Journal of Spacecraft and Rockets*, Vol. 10, No. 2, Feb. 1973, pp. 126–132.

[6] Spencer, T. M., "Attitude Dynamics of a 'Nearly-Spherical' Dual-Spin Satellite and Orbital Results for OSO-7," 13th Congress of the International Union of Theoretical and Applied Mechanics, Moscow, Aug. 1972.

[7] *Proceedings of the Symposium on Attitude Stabilization and Control of Dual-Spin Spacecraft*, Air Force Rept. SAMSO-TR-68-191, Aug. 1967, El Segundo, Calif.

[8] Martin, E. R., "Fuel Slosh and Dynamic Stability of Intelsat IV," AIAA Paper 71-954, Hempstead, N.Y., 1971.

[9] O'Hern, E. A., Baddeley, V., and Rakowski, J. E., "Analysis of Effects of Fluid Energy Dissipation on Spinning Satellite Control Dynamics," AIAA Paper 72-886, Stanford, Calif., 1972.

[10] Scher, M. P., "Effects of Flexibility in the Bearing Assemblies of Dual-Spin Spacecraft," *AIAA Journal*, Vol. 9, No. 5, May 1971, pp. 900–909.

[11] Likins, P. W., Tseng, G., and Mingori, D. L., "Stable Limit Cycles Due to Nonlinear Damping in Dual-Spin Spacecraft, *Journal of Spacecraft and Rockets*, Vol. 8, No. 6, June 1971, pp. 568–574.

[12] Spencer, T. M., "Cantilevered-Mass Nutation Damper for a Dual-Spin Spacecraft," Air Force Rept. SAMSO-TR-68-191, Aug. 1967, El Segundo, Calif.

[13] Thompson, W. T., *Introduction to Space Dynamics*, Wiley, New York, 1961, pp. 214–216.